Materials and Structures (2010) 43:803–814
DOI 10.1617/s11527-009-9549-0

ORIGINAL ARTICLE

Development of engineered cementitious composites with limestone powder and blast furnace slag

Jian Zhou · Shunzhi Qian · M. Guadalupe Sierra Beltran · Guang Ye · Klaas van Breugel · Victor C. Li

Received: 28 January 2009 / Accepted: 11 August 2009 / Published online: 17 September 2009

Abstract Nowadays limestone powder and blast furnace slag (BFS) are widely used in concrete as blended materials in cement. The replacement of Portland cement by limestone powder and BFS can lower the cost and enhance the greenness of concrete, since the production of these two materials needs less energy and causes less CO_2 emission than Portland cement. Moreover, the use of limestone powder and BFS improves the properties of fresh and hardened concrete, such as workability and durability. Engineered cementitious composites (ECC) is a class of ultra ductile fiber reinforced cementitious composites, characterized by high ductility, tight crack width control and relatively low fiber content. The limestone powder and BFS are used to produce ECC in this research. The mix proportion is designed experimentally by adjusting the amount of limestone powder and BFS, accompanied by four-point bending test and uniaxial tensile test. This study results in an ECC mix proportion with the Portland cement content as low as 15% of powder by weight. This mixture, at 28 days, exhibits a high tensile strain capacity of 3.3%, a tight crack width of 57 μm and a moderate compressive strength of 38 MPa. In order to promote a wide use of ECC, it was tried to simplify the mixing of ECC with only two matrix materials, i.e. BFS cement and limestone powder, instead of three matrix materials. By replacing Portland cement and BFS in the aforementioned ECC mixture with BFS cement, the ECC with BFS cement and limestone powder exhibits a tensile strain capacity of 3.1%, a crack width of 76 μm and a compressive strength of 40 MPa after 28 days of curing.

Keywords Engineered cementitious composites · Tensile strain capacity · Limestone powder · Blast furnace slag · Blast furnace cement

J. Zhou (✉) · S. Qian · M. G. Sierra Beltran · G. Ye · K. van Breugel
Microlab, Faculty of Civil Engineering and Geosciences, Delft University of Technology, Delft, The Netherlands
e-mail: Jian.Zhou@tudelft.nl

S. Qian
e-mail: s.qian@tudelft.nl

M. G. Sierra Beltran
e-mail: m.g.sierrabeltran@tudelft.nl

G. Ye
e-mail: g.ye@tudelft.nl

K. van Breugel
e-mail: k.vanbreugel@tudelft.nl

G. Ye
Magnel Laboratory for Concrete Research, Department of Structural Engineering, Ghent University, Technologiepark-Zwijnaarde 904, Zwijnaarde, Ghent 9052, Belgium

V. C. Li
ACE-MRL, Department of Civil and Environmental Engineering, University of Michigan, Ann Arbor, MI, USA
e-mail: vcli@engin.umich.edu

Abbreviations

ECC	Engineered cementitious composites
PVA	Polyvinyl alcohol
BFS	Blast furnace slag
$CaCO_3$	Calcium carbonate
ESEM	Environmental scanning electron microscopy
BSE	Backscattered electron
PC/BFS	Portland cement-to-BFS

1 Introduction

ECC, short for engineered cementitious composites, is a class of ultra ductile fiber reinforced cementitious composites originally invented at the University of Michigan in the early 1990s [1]. This group of materials is characterized by high ductility in the range of 3–7%, tight crack width of around 60 μm and relatively low fiber content of 2% or less by volume. Figure 1 shows a typical tensile stress–strain curve of ECC and its tight crack width control [2]. Unlike plain concrete and fiber reinforced concrete, ECC shows a metal-like property after the first cracking. This unique tensile strain-hardening behavior results from an elaborate design using a micromechanics model taking into account the interactions among fiber, matrix and fiber-matrix interface [3].

The fiber-matrix interface properties play a very important role on the tensile strain-hardening behavior of ECC. The typical fiber used in ECC is the polyvinyl alcohol (PVA) fiber with a diameter of 39 μm and a length of 6–12 mm. The PVA fiber shows a slip-hardening behavior when pulling out of cement-based matrix as shown in Fig. 2 [4]. After the fiber-matrix completes debonding, accompanied by the drop after the first load peak in the single fiber pullout curve, the frictional bond between the fiber and the matrix increases as the fiber slips out of the matrix. The fiber can be completely pulled out from the matrix, when the embedment length is small. The fiber ruptures, when the embedment length is large. When ECC is loaded in tension, the matrix starts to crack in its weakest cross-section. The fibers crossing this crack take over the tensile load. As the fibers slip out of the matrix, the crack progressively opens. Due to the slip-hardening behavior of fibers, ECC can carry an increasing load, which generates new cracks at other sites. By repeating this process ECC exhibits multiple-cracking behavior and, therefore, strain-hardening behavior. Fiber rupture is limited by crack width control attained by a steady state flat crack propagation mode [4].

The crack width of ECC determines the transport of water and harmful substance, such as Cl^-, SO_4^{2-}, and CO_2. ECC has a tight crack width self-controlled to around 60 μm without the presence of steel reinforcement. This is much smaller than the typical crack width observed in the steel reinforced concrete and the fiber reinforced concrete. Therefore, ECC shows a lower water permeability and a better durability compared with conventional concrete. An experimental study [5]

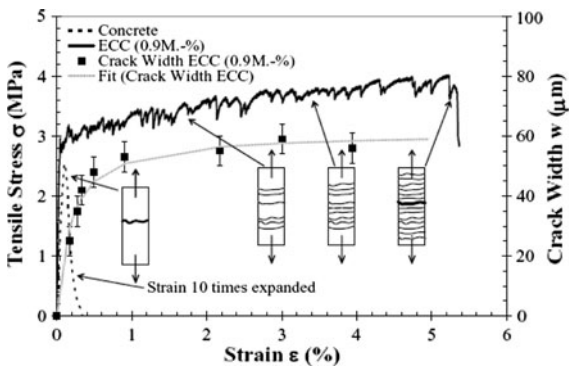

Fig. 1 Tensile stress–strain curve and tight crack width control of ECC [2]

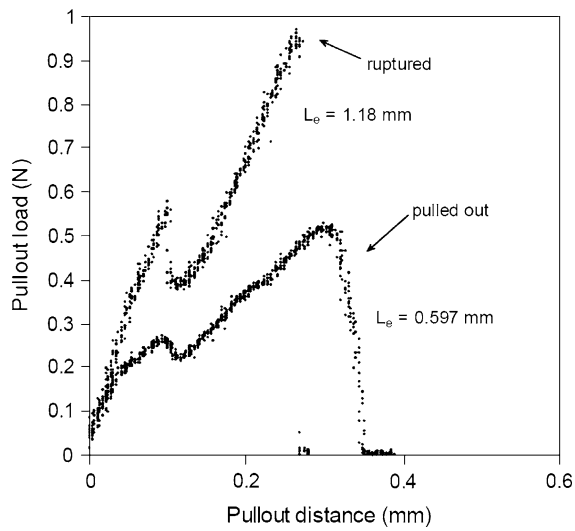

Fig. 2 Single fiber pullout curves of PVA fiber with the diameter of 39 μm [4]

revealed that under the same pre-tension deformation of 1.5%, the crack width of ECC was much smaller than that of the steel reinforced mortar, and ECC had a water permeability several orders of magnitude lower than the steel reinforced mortar. It was also reported [6] that ECC can significantly enhance the durability of structures exposed to aggressive environments, such as freeze–thaw cycles, hot water immersion, chloride immersion, deicing-salt exposure and alkali-silicate reaction. The use of ECC can prolong the service life of structures and reduce the maintenance and repair costs. Therefore, the use of ECC lowers the life cycle cost of structures, although ECC costs two to three times higher than conventional concrete [7]. Nowadays ECC is emerging in broad applications, such as ECC link slab on bridge decks [8], ECC coupling beam in high-rise buildings to enhance their seismic resistance, composite ECC/steel bridge deck and some concrete repair applications [9].

This paper presents the research, conducted at Microlab in Delft University of Technology, aimed to develop a new version of ECC with locally available materials. Portland cement, limestone powder and blast furnace slag (BFS) are used to produce ECC as matrix materials. Limestone powder is produced by finely grinding limestone and consists principally of calcium carbonate ($CaCO_3$). Since only a small amount of limestone powder reacts with cement clinker or hydration products, it is usually considered as an inert filler material [10]. The incorporation of limestone powder with Portland cement has many advantages on early compressive strength, durability and workability [11]. BFS is a by-product in the manufacture of pig iron, and it is the main cement replacement material in the Netherlands. Due to the amorphous glassy-like microstructure consisting of mono-silicates, BFS shows a potential of pozzolanic reaction [12]. When mixed with Portland cement, BFS accelerates the hydration of Portland cement and reacts with the calcium hydroxide, one of the hydration products of Portland cement. Although the addition of BFS results in a lower strength at early age, the replacement of Portland cement by BFS, up to 70%, does not have any negative effect on the compressive strength of concrete after 28 days [13]. The addition of BFS can improve the durability of concrete, for instance, enhancing sulfate attack resistance and decelerating chloride ion penetration. Besides, the addition of BFS results in a more homogeneous fiber distribution, because BFS particles provide a driving force for fiber dispersion [14]. Therefore, the use of limestone powder and BFS in ECC not only reduces the cost and increases the greenness, but also improves the workability, the mechanical properties and the durability of ECC.

Table 1 Compositions of BFS cements [15]

Types of BFS cement	Clinker (%)	BFS (%)	Minor additional constituents (%)
CEM III/A	35–64	36–65	0–5
CEM III/B	20–34	66–80	0–5
CEM III/C	5–19	81–95	0–5

Furthermore, in order to promote a wide use of ECC, it is tried to simplify the mixing of ECC with only two matrix materials, i.e. BFS cement and limestone powder, instead of three matrix materials. The BFS cement is used to replace Portland cement and BFS in ECC mixtures. The BFS cement is produced by mixing Portland cement clinker and BFS and then grinding them together. According to different BFS contents, the family of the BFS cements can be divided into three types, i.e. CEM III/A, CEM III/B and CEM III/C [15]. Table 1 gives the composition of the three types of BFS cements.

Firstly, the ECC mix design with Portland cement, limestone powder and BFS is discussed. The experimental results of four-point bending test, uniaxial tensile test, loaded crack width measurement and compressive test are reported. Then the images captured under environmental scanning electron microscopy (ESEM) are employed to explain the microstructural properties of ECCs. Finally, the development of the ECC mixed with BFS cement and limestone powder is presented.

2 Experimental program

2.1 Materials

Two groups of matrix materials were used to produce ECC. The first group included Portland cement CEM I 42.5 N, limestone powder and BFS. The mix proportion of a standard ECC mixture M45 (Table 2) [16] is used as a reference in the ECC mix design. Table 3 gives the mix proportion of the ECC mixtures mixed with the first group of matrix materials. The second

Table 2 Mix proportion of ECC mixture M45 (weight %) [16]

Mix number	Type I cement	Silica sand	Fly ash	Water/powder ratio	Super-plasticizer	PVA fiber (by volume)
M45	1	0.8	1.2	0.2	0.013	2%

Table 3 Mix proportion of the ECCs with Portland cement, limestone powder and BFS (weight %)

Mix Number	CEM I 42.5 N	Limestone powder	BFS	Water/powder ratio	Super-plasticizer	PVA fiber (by volume, %)
M1	1	0.8	1.2	0.27	0.025	2
M2	1	1.5	1.2	0.27	0.023	2
M3	1	2	1.2	0.26	0.018	2
M4	1	3	1.2	0.26	0.018	2
M5	1	2	1	0.26	0.018	2
M6	0.6	2	1.4	0.26	0.020	2

Table 4 Mix proportion of the ECC mixture mixed with BFS cement and limestone powder (weight %)

CEM III/B 42.5 N (g)	Limestone powder (g)	Water/powder ratio	Super-plasticizer (g)	PVA fiber (by volume)
1	1	0.26	0.020	2%

Table 5 Chemical compositions of CEM I 42.5 N, limestone powder, BFS and CEM III/B 42.5 N

Compound	CEM I 42.5 N (%)	Limestone powder (%)	BFS (%)	CEM III/B 42.5 N (%)
CaO	64.1	–	40.8	47
SiO_2	20.1	0.3	35.4	30
Al_2O_3	4.8	0.1	13	9
Fe_2O_3	3.2	0.1	0.5	1
MgO	–	0.2	8.0	–
K_2O	0.5	–	0.5	–
Na_2O	0.3	–	0.2	–
SO_3	2.7	–	0.1	3.2
$CaCO_3$	–	98.8	–	–

The chemical compositions of CEM I 42.5 N, limestone powder and CEM III/B 42.5 N were from the manufacturers, and that of BFS was measured by energy dispersive X-ray analysis

group included BFS cement and limestone powder. The experimental study revealed that among the first group of ECC mixtures, M6, in which the Portland cement-to-BFS (PC/BFS) ratio was 0.43, showed the best mechanical properties. Since the ratio of 0.43 matches the typical value in BFS cements CEM III/B, the BFS cement CEM III/B 42.5 N was used in this study. Table 4 gives the mix proportion of the ECC mixture mixed with CEM III/B 42.5 N and limestone powder. The chemical compositions of CEM I 42.5 N, limestone powder, BFS and CEM III/B 42.5 N are given in Table 5. The densities of CEM I 42.5 N, limestone powder, BFS and CEM III/B 42.5 N are 3150 kg/m^3, 2700 kg/m^3, 2850 kg/m^3 and 2960 kg/m^3, respectively. Figure 3 shows the particle size distribution curves of CEM I 42.5 N, limestone powder, BFS and CEM III/B 42.5 N, which were measured with laser-diffraction technique. The mean particle sizes of CEM I 42.5 N, limestone powder, BFS and CEM III/B 42.5 N are 16.2, 13.4, 10.6 and 10.7 μm, respectively. In all mixtures, the fiber content was 2% by volume. The fiber used in this study was the PVA fiber with a

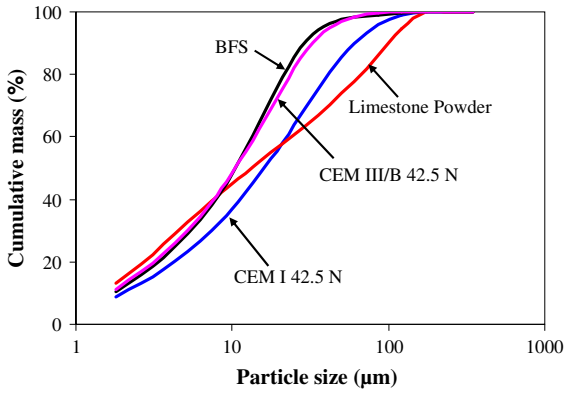

Fig. 3 Particle size distribution of CEM I 42.5 N, limestone powder, BFS and CEM III/B 42.5 N, measured with laser-diffraction technique

length of 8 mm and a diameter of 40 μm. The tensile strength of the PVA fiber is 1600 MPa and the density is 1,300 kg/m^3. The fiber surface is coated with 1.2% oil by weight to reduce the fiber-matrix chemical and friction bond.

2.2 Mixing and curing

The matrix materials were first mixed with a HOBART® mixer for 1 min at low speed. Then water and superplasticizer were added at low speed mixing. Mixing continued at low speed for 1 min and then at high speed for 2 min. After fibers were added, the sample was mixed at high speed for another 2 min.

The fresh ECC was cast into six coupon specimens with the dimension of 240 mm × 60 mm × 10 mm and a prism with the dimension of 160 mm × 40 mm × 40 mm. After 1 day curing in moulds covered with plastic paper, the specimens were demoulded and cured under sealed condition at a temperature of 20°C for another 27 days.

2.3 Four-point bending and compressive tests

After 28-day curing, the coupon specimens were sawn into four pieces with the dimension of 120 mm × 30 mm × 10 mm. These specimens were used in four-point bending test. The support span of the four-point bending test set-up was 110 mm, and the load span was 30 mm as shown in Fig. 4. Two LVDTs were fixed on both sides of the test set-up to measure the flexural deflection of the specimen. The test was conducted under deformation control at the speed of 0.01 mm/s. Three measurements were done for each mixture.

After 28 days of curing, the prism specimens were sawn into three cubes with the dimension of 40 × 40 × 40 mm^3. These cubes were used for compressive tests. Three measurements were done for each mixture.

2.4 Uniaxial tensile test

A uniaxial tensile test set-up was developed for ultra ductile fiber reinforced concrete, such as ECC, as shown in Fig. 5. The specimen is clamped by four steel plates, one pair at each end. Each pair of steel plates is tightened with four bolts. Two pairs of steel plates are fixed on the loading device with four steel bars, two for each pair. Between the pairs of steel plates and the loading device, there is a ± 3 mm allowance. It is used to diminish the eccentricity in the direction perpendicular to the plate of the specimen by moving the steel plates along the steel bar. The tensile force is transferred to the specimen by the friction force between the steel plates and the specimen. Four aluminum plates, 1 mm thick each, are glued on both sides of the ends of specimen in order to improve the friction force, to ensure the clamped area work together and to prevent the local damage on the specimen caused by high clamping force.

Fig. 4 Four-point bending test set-up

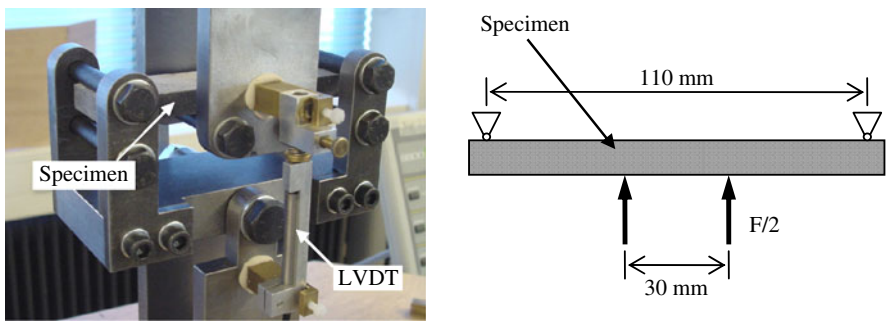

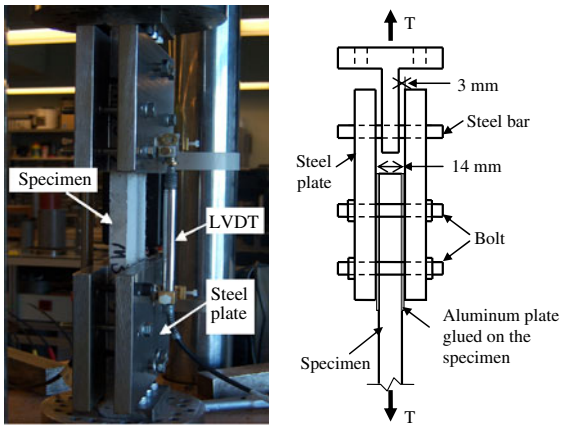

Fig. 5 Uniaxial tensile test set-up

The experimental procedure is described in details hereafter. The coupon specimens were sanded to obtain a flat surface with a larger bond strength with the aluminum plates. After cleaning the specimen surface and the aluminum plate with Acetone, the aluminum plates were glued on the specimen. The glue was cured for 1 day before testing. Before placing the specimen in the test set-up, two pairs of steel plates were connected to the bottom and the top parts of loading device, respectively. The lower end of the specimen was first clamped with the steel plates by tightening four bolts. Then the upper end of the specimen was clamped with the other pair of steel plates. Finally, two LVDTs were mounted on both sides of the specimen. The testing gauge length was 70 mm. The tests were conducted under deformation control with a loading speed of 0.005 mm/s. More than four specimens were tested for each mixture.

How to alleviate eccentricity is of most concern in uniaxial tensile testing. The eccentricity can lead to a bending moment in the cross-section of the testing specimen and therefore an uneven stress distribution. The larger the eccentricity is, the larger the bending moment is. With large bending moment imposed on the specimen, cracking starts on the side of the specimen with high tensile stress, even when the average stress in this cross-section is lower than the tensile strength. The crack can quickly propagate into the specimen, due to the stress localization at the crack front and the loss of cross sectional area. As a result, the measured tensile strength and strain capacity appears far from true uniaxial tensile properties.

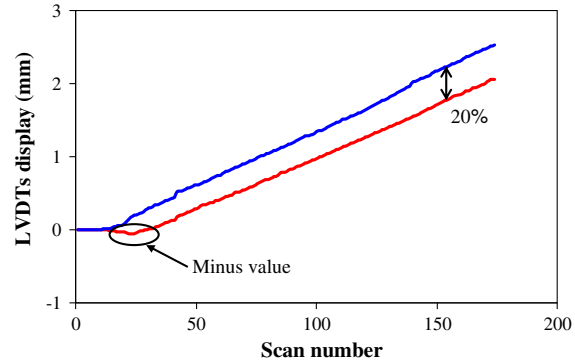

Fig. 6 A case with large difference between the measurements of two LVDTs indicating there was a large eccentricity on the measured specimen

In this study, two LVDTs attached on both sides of the specimen were used to measure the eccentricity in the direction perpendicular to the plane of the coupon specimen. If eccentricity exists, the deformations measured with LVDTs on two sides of the specimen will be different. The difference between the deformations on two sides is proportional to the eccentricity. Figure 6 presents a case of a large eccentricity. At the beginning of the measurement, it was observed that one side of the specimen was under compression indicated by the negative value in the lower curve while the other side was under tension indicated by the positive value. At the later stage, a 20% difference between the measurements of two LVDTs was observed. This case occurred in the development stage of the test set-up. After some modification, the difference between the two LVDTs displays decreased to less than 10%. Note that the distance between the two LVDTs was around 40 mm, which was four times the thickness of the specimen. Therefore, the difference of the deformations between the two sides of the specimen was a quarter of the difference between the two LVDTs, and the maximum difference of the deformations between two sides of the specimen was 2.5%.

2.5 Loaded crack width measurement

The crack width was measured on the coupon specimens after the uniaxial tensile test. Three lines parallel to the loading direction were drawn on the specimen. These lines were uniformly spaced on the width of specimen as shown in Fig. 7. Under microscope, the number of cracks crossing each line

Fig. 7 Illustration of the measurement of loaded crack width

was counted. The average crack number of each specimen was calculated by averaging the number of cracks crossing these three lines. Since ECC deforms several hundred times larger than the matrix, the tensile deformation of the matrix contributes little to the overall tensile deformation of ECC. Therefore, the overall tensile deformation of ECC can be related only to the crack opening. Accordingly, the average crack width w can be calculated by dividing the measured tensile deformation at the peak load Δl by the average crack number N, viz:

$$w = \frac{\Delta l}{N} \tag{1}$$

The calculated crack width is the *loaded* crack width. This is different from the residual crack width in the previous studies [17], in which the crack width is measured after partial crack closure due to the relaxation after unloading. According to Yang et al. [17], the loaded crack width is roughly twice of the residual crack width.

2.6 ESEM observation

The ESEM study was conducted to investigate the microstructural properties of ECC. After the four-point bending test, the specimens were freeze-dried. The dried specimens were placed in a vacuum chamber and impregnated with a low-viscosity epoxy. After the hardening of epoxy, the specimens were carefully ground on the middle-speed lap wheel with p120, p220, p320, p500, p1200 and p4000 sand papers and were then polished on the lap wheel with 6, 3, 1 and 0.25 μm diamond pastes. The final polishing was done with a low-relief polishing cloth. Each grinding and polishing step took 2 min. The images were taken on the prepared section using a backscattered electron (BSE) detector with vapor mode. The acceleration voltage of 20 kV was used in order to obtain a high contrast image.

3 Results and discussion

3.1 ECC mixed with Portland cement, limestone powder and BFS

The mix proportion of a standard ECC mixture M45 with Portland cement, silica sand and fly ash [16] is used as a reference in the ECC mix design with Portland cement, limestone powder and BFS. When blended with Portland cement, limestone powder and silica sand behave as inert materials. However, BFS and fly ash have a potential of pozzolanic reaction and these reactions need to be activated by the hydration products of Portland cement. In mix design, Portland cement and BFS are considered as cementitious materials, and limestone powder is considered as inert filler material. Table 3 gives the mix proportion of the ECC mixtures mixed with different limestone powder and BFS contents. M1 is a trial mixture, and its mix proportion comes from that of M45 with replacing silica sand and fly ash by limestone powder and BFS, respectively. A higher water-to-powder ratio is used because of the higher water demand of BFS compared with fly ash. The ECC mix design is divided into two steps. Firstly, the mixtures M1-4 are used to investigate the effect of limestone powder and to find out the optimum limestone powder content. Limestone powder with a mean particle size of 13.4 μm has a smaller particle size than the silica sand used in M45 with a mean particle size of 110 μm [17]. The small particle of limestone powder results in a decrease in the matrix toughness, which is conducive to a high tensile strain capacity [3]. Therefore, increasing limestone powder contents are used in the mixtures M1-4. In order to obtain good workability, the water-to-powder ratio and the superplasticizer content decrease slightly from M1 to M4. Among these four mixtures, M3, in which the cementitious materials-to-limestone powder ratio is 1.1, exhibits the highest tensile strain capacity. Then, the cementitious materials-to-limestone powder ratio of 1.0 is used in M5 and M6. In these two mixtures, the PC/BFS ratios of 1.0 and 0.43 are used, since these two ratios match the typical values in BFS cements CEM III/A and CEM III/B, respectively.

3.1.1 *Flexural and uniaxial tensile performance*

Under four-point bending load and uniaxial tensile load, the mixtures M1-6 all exhibit multiple-cracking behavior as shown in Fig. 8. Among the six mixtures, M6 shows the best flexural and tensile properties. However, M6 has the lowest cement content of 15% of powder materials by weight, which is more or less the same as the cement content in normal concrete. Figure 9 shows the flexural load–deflection curves and the tensile stress–strain curves of M6. In the flexural load–deflection curves, the maximum flexural stress is defined as the flexural strength, and the corresponding deflection is defined as the flexural deflection capacity. In the tensile stress–strain curves, the stress at the first drop associated with the first cracking is defined as the first cracking strength. Similarly, the maximum stress is defined as the ultimate tensile strength, and the corresponding strain is defined as the tensile strain capacity. The flexural deflection capacity and tensile strain capacity of M6 can be calculated by averaging the results of three-four-point bending measurements and four uniaxial tensile measurements, and they are 3.9 mm and 3.3%, respectively.

The flexural deflection capacity and the tensile strain capacity of ECCs with different limestone powder contents and BFS contents are summarized in Fig. 10 and Table 6. The results of the four-point bending test and the uniaxial tensile test indicate a linear correlation between the flexural deflection capacity and the tensile strain capacity as shown in

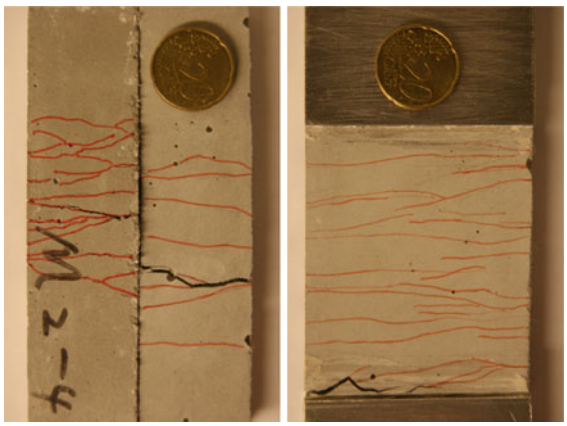

Fig. 8 Multiple cracking of the specimens under four-point bending load (*left*) or uniaxial tensile load (*right*)

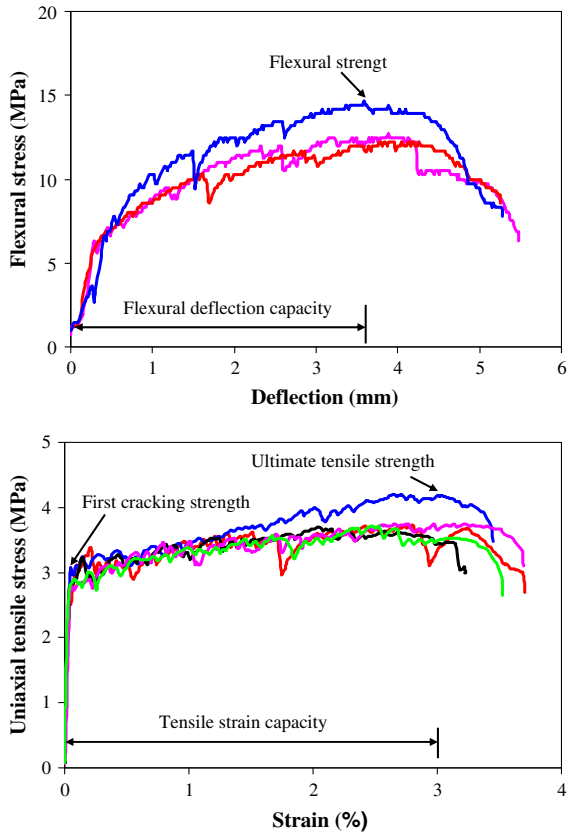

Fig. 9 Flexural load–deflection curves (*above*) and tensile stress–strain curves (*below*) of M6 with the average flexural deflection capacity of 3.9 mm and the average tensile strain capacity of 3.3%

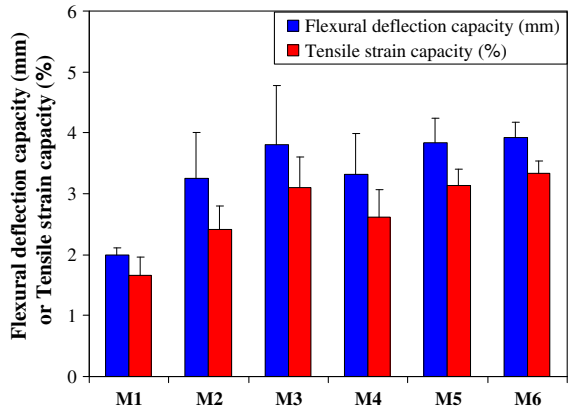

Fig. 10 Flexural deflection capacity and tensile strain capacity of ECCs at 28 days

Fig. 11, as was suggested from ECC flexural beam analysis [16, 18]. For these six mixtures (M1-6) mixed and cured at different times, the standard

Table 6 Flexural deflection capacity and tensile strain capacity of ECCs at 28 days

Mixture	M1	M2	M3	M4	M5	M6
Flexural deflection capacity (mm)	2.0 ± 0.1	3.2 ± 0.8	3.8 ± 1.0	3.3 ± 0.7	3.8 ± 0.4	3.9 ± 0.3
Tensile strain capacity (%)	1.7 ± 0.3	2.4 ± 0.5	3.1 ± 0.6	2.6 ± 0.5	3.1 ± 0.3	3.3 ± 0.2

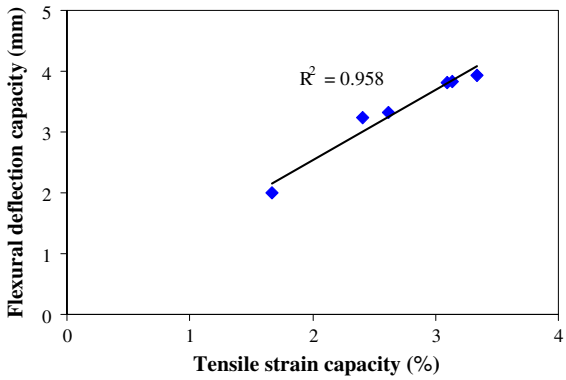

Fig. 11 Correlation between the tensile strain capacity and the flexural deflection capacity

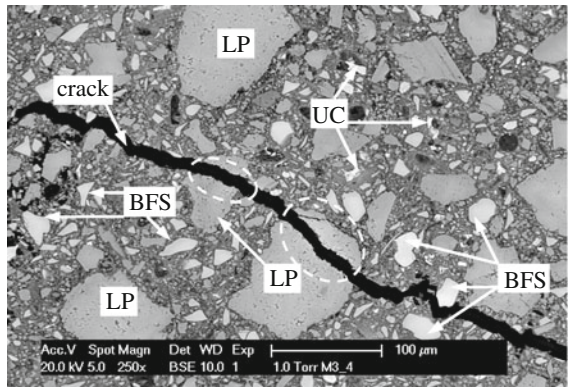

Fig. 12 BSE image of M3 at 28 days shows a crack crossing the limestone powder particles. Here, LP indicates limestone powder particle and UC indicates the anhydrate cement particles

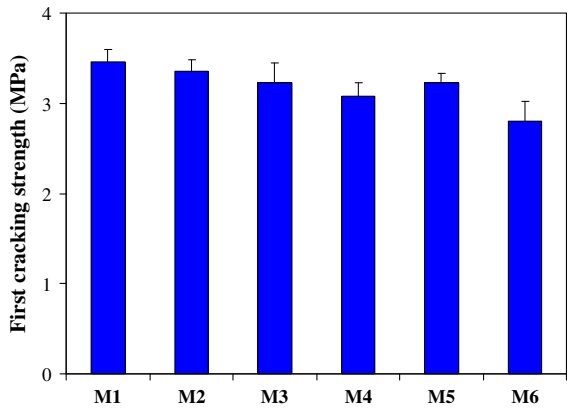

Fig. 13 First cracking strength of ECCs from uniaxial tensile test at 28 days

deviations of the tensile strain capacity within each mix design are lower than 0.6%, which is <20% of the tensile strain capacity. It can be concluded that the newly developed uniaxial tensile test set-up can give relatively consistent results, and the material properties of ECCs with limestone powder and BFS are relatively robust.

For the mixtures M1-4, as the limestone powder content increases, the flexural deflection capacity and the tensile strain capacity first increase and then decrease. The flexural deflection capacity and the tensile strain capacity are in the same order from large to small: M3, M4, M2 and M1. Although M1 exhibits the smallest deformation capacity, its tensile strain capacity is already as high as 1.7%, which is much higher than that of conventional concrete (about 0.01%). Since the limestone powder behaves as inert filler materials, the addition of limestone powder results in a lower tensile strength of the matrix. Besides, due to the low hardness of limestone powder, the large limestone powder particle is easy to break, and the crack crosses the big limestone powder particles (Fig. 12). Therefore, the addition of the limestone powder results in the decrease in the toughness of the matrix, reflected by the decrease in the first cracking strength as shown in Fig. 13. The decreasing matrix toughness is conducive to the high ductility of the ECC composite [3]. On the other hand, too much addition of limestone powder leads to a weak fiber-matrix interface. Li [19] suggested that excessively weak interface has a negative effect on the strain-hardening behavior of ECC. The experimental results reveal that M3 has the optimum limestone powder content in terms of deformation capacity.

As shown in Fig. 10, both M5 and M6 show a tensile strain capacity higher than 3%. The decrease in the PC/BFS ratio results in the increase in the flexural deflection capacity and in the increase in the

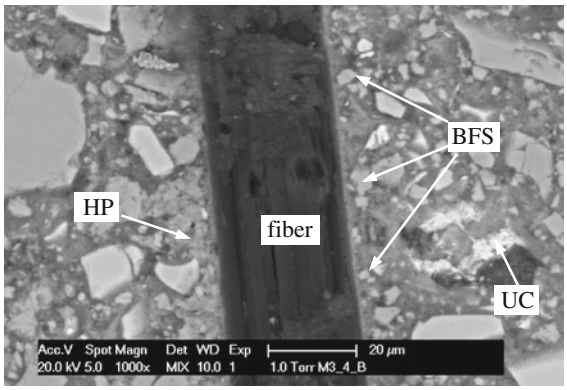

Fig. 14 BSE image showing the fiber-matrix interface. Here, HP indicates hydration products and UC indicates the anhydrate cement particles

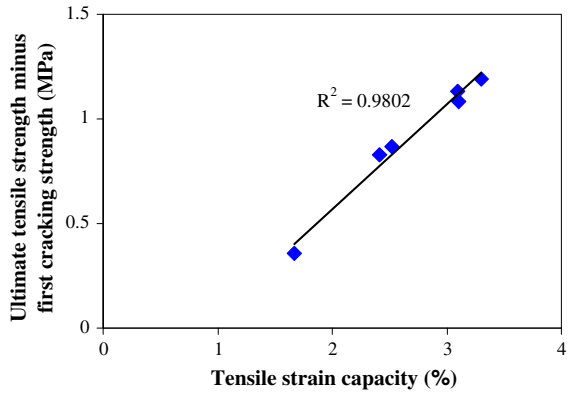

Fig. 15 Correlation between the tensile strain capacity and the margin between the ultimate tensile strength and the first cracking strength

tensile strain capacity. This can be attributed to the lower matrix toughness and the better fiber-matrix interface due to the addition of BFS. In mixture M5 and M6, as the BFS content increases, the first cracking strength decreases as shown in Fig. 13, and therefore the toughness of the matrix decreases. A dense matrix-fiber interface is observed under ESEM as shown in Fig. 14. Lots of small BFS particles pack in the interface. Little calcium hydroxide at the interface is observed. Instead, the most observed hydration product at the interface is C–S–H, which has a relatively denser structure and better friction bond with the fiber.

The multiple cracking behavior of ECC results from the interaction among fiber, matrix and interface. One of the criteria for having the multiple-cracking behavior is that the matrix tensile strength must be lower than the fiber bridging strength across the crack plane [19]. Consequently, after the matrix cracks, the fibers can carry the increasing tensile load, which generates new cracks. When the tensile load exceeds the minimum fiber bridging strength in ECC, the fibers in this crack plane are pulled out of the matrix or rupture, and ECC fails. The minimum fiber bridging strength is recorded as the ultimate tensile strength in the uniaxial tensile test. Obviously, a larger margin between the ultimate tensile strength and the first cracking strength gives the matrix more chances to crack and results in a higher tensile strain capacity. The experimental results confirm this, and the tensile strain capacity shows a strong relation with the margin between the ultimate tensile strength and the first cracking strength as shown in Fig. 15.

3.1.2 *Loaded crack width*

The loaded crack width of ECC determines the transport properties in the loaded state, and therefore it is a crucial parameter for the durability of ECC. Figure 16 shows the loaded crack width of the ECCs with limestone powder and BFS. All mixtures show a loaded crack width smaller than 100 μm. Among six mixtures M6 shows a very tight crack width of 57 μm. It can be expected that M6 has relatively low water permeability and good durability.

The increasing limestone powder and BFS contents lead to a smaller loaded crack width. As shown in Fig. 3, limestone powder and BFS have higher contents of small particles ranging from 1 to 10 μm than Portland cement. The higher contents of small particles result in a better packing at the fiber-matrix

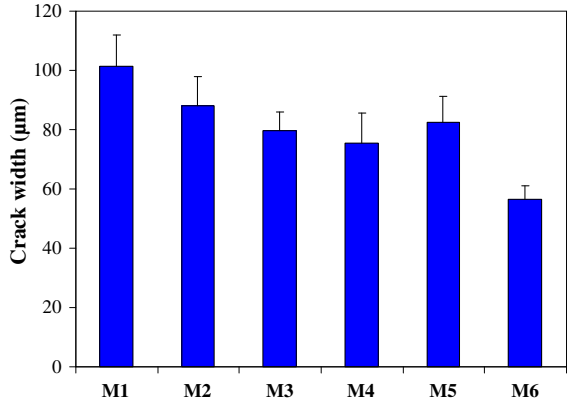

Fig. 16 Loaded crack width of ECCs at 28 days

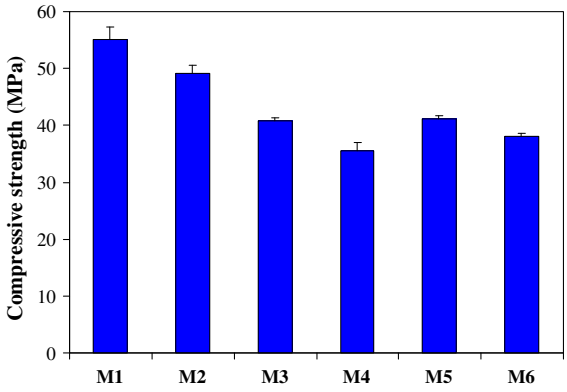

Fig. 17 Compressive strength of ECCs at 28 days

interface and in a better interfacial property. For M4, the low ultimate tensile strength results in a small fiber slipping out of the matrix. As a result, the crack width is small.

3.1.3 Compressive strength

The compressive strength of the ECCs at 28 days is summarized in Fig. 17. The increasing limestone powder content results in a decrease in the compressive strength in M1-4. Comparing the compressive strength of mixtures M5 and M6, the high cement replacement by BFS causes little decrease in the compressive strength. The mixtures M3, M5 and M6 with good tensile property all show compressive strengths higher than 38 MPa. This value can fulfill engineering requirements in most projects.

3.2 ECC mixed with BFS cement and limestone powder

In order to promote a wide use of ECC, it is tried to further simplify the mixing of ECC with only two matrix materials instead of three, i.e. BFS cement is used to replace Portland cement and BFS. The experiment reveals that M6, which has the PC/BFS ratio of 0.43, exhibits the highest tensile strain capacity among the six mixtures. The PC/BFS ratio of 0.43 is approximately the same as that in BFS cement CEM III/B 42.5 N, in which the clinker content is 29%, and the BFS content is 71%. Therefore, the BFS cement CEM III/B 42.5 N is used to produce ECC with limestone powder. Table 4 gives the mix proportion of ECC, which comes from the mix proportion of M6 by replacing Portland cement CEM I 42.5 N and BFS by BFS cement CEM III/B 42.5 N. At 28 days, this mixture shows a tensile strain capacity of 3.1% and a compressive strength of 40 MPa, in general agreement with M6. The loaded crack width of this mixture is 76 μm, which is larger than that of M6 of 57 μm. This may be because of the difference between particle size distributions of BFS in the interground CEM III/B 42.5 N and the blended M6 [20].

4 Conclusions

A set of ECCs was developed with Portland cement CEM I 42.5 N, limestone powder and BFS. The mix proportion was designed experimentally by adjusting the amount of limestone powder and BFS, accompanied by four-point bending test and uniaxial tensile test. The loaded crack width and the compressive strength were also measured. ESEM study was used to investigate the microstructure of ECCs. Furthermore, a ECC mixture with BFS cement and limestone powder was developed and evaluated with experiments in order to reduce the matrix materials from three to two and thus to simplify the mixing of ECC. The following conclusions can be drawn from the experimental study:

1. Under four-point bending load and uniaxial tensile load, all specimens exhibit multiple-cracking behavior. For the six mixtures with different limestone powder and BFS contents, the flexural deflection capacity ranges from 2.0 to 3.9 mm, and the tensile strain capacity ranges from 1.7 to 3.3% at 28 days. It is found that there is a strong correlation between the tensile strain capacity and the margin between the ultimate tensile strength and the first cracking strength. As the margin increases, the tensile strain capacity increases.
2. As the limestone powder content increases, the flexural deflection capacity and the tensile strain capacity first increase and then decrease. With the same limestone powder content, as the cement replacement by BFS increases from 50 to 70%, the flexural deflection capacity and the tensile strain capacity increase.
3. The increasing limestone powder and BFS contents lead to a smaller average loaded crack

width. All mixtures show a average loaded crack width smaller than 100 μm.

4. The experimental study results in an ECC mix proportion with a Portland cement content as low as 15% of powder by weight. This mixture, at 28 days, shows high tensile strain capacity of 3.3%, a moderate compressive strength of 38 MPa and a tight crack width of 57 μm.
5. In order to simplify the mixing of ECC, BFS cement is used to replace Portland cement and BFS. The ECC mixed with BFS cement CEM III/B 42.5 N and limestone powder has the properties in agreement with the ECC mixture with Portland cement, limestone powder and BFS.

Acknowledgments This research is financially supported by the Delft Clusters and Heijmans Infrastructure B.V. Their support is gratefully acknowledged. We would like to thank BAS B.V. for their help in measuring the particle size distribution of powder materials. V.C. Li would like to acknowledge the US National Science Foundation CI-Team grant OCI 0636300 for supporting international research collaboration.

References

1. Li VC (1993) From micromechanics to structural engineering–the design of cementitious composites for civil engineering applications. JSCE J Struct Mech Earthq Eng 10(2):37–48
2. Weimann MB, Li VC (2003) Hygral behavior of engineered cementitious composite (ECC). Int J Restor Build Monum 9(5):513–534
3. Li VC, Leung CKY (1992) Theory of steady state and multiple cracking of random discontinuous fiber reinforced brittle matrix composites. J Eng Mech 118(11):2246–2264
4. Yang EH, Wang S, Yang Y, Li VC (2008) Fiber-bridging constitutive law of engineered cementitious composites. J Adv Concr Tech 6(1):181–193
5. Lepech MD, Li VC (2005) Water permeability of cracked cementitious composites. In: Carpinteri A (ed) Proceedings of the 11th international conference on fracture, Turin, Italy, 20–25 March 2005, Paper 4539
6. Li VC (2007) Engineered cementitious composites (ECC)—material, structural and durability performance. In: Nawy E (ed) Concrete construction engineering handbook, CRC Press, Boca Raton, Chapter 24
7. Keoleian GA, Kendall A, Dettling JE, Smith VM, Chandler RF, Lepech MD, Li VC (2005) Life cycle modeling of concrete bridge design: Comparison of engineered cementitious composite link slabs and conventional steel expansion joints. ASCE J Infrastruct Syst 11(1):51–60
8. Michigan DOT (2005) Bridge decks going jointless: Cementitious composites improve durability of link slabs. Constr Tech Res Rec 100:1–4
9. Kunieda M, Rokugo K (2006) Recent progress on HPFRCC in Japan. J Adv Concr Tech 4(1):19–33
10. Poppe AM, De Schutter G (2005) Cement hydration in the presence of high filler contents. Cem Concr Res 35(12):2290–2299
11. Tsivilis S, Batis G, Chaniotakis E, Grigoriadis G, Theodossis D (2000) Properties and behavior of limestone cement concrete and mortar. Cem Concr Res 30(10):1679–1683
12. Bijen J (1996) Benefits of slag and fly ash. Constr Build Mater 10(5):309–314
13. Swaddiwudhipong S, Lu HR, Wee TH (2003) Direct tension test and tensile strain capacity of concrete at early age. Cem Concr Res 33(12):2077–2084
14. Kim JK, Kim JS, Ha GJ, Kim YY (2007) Tensile and fiber dispersion performance of ECC (engineered cementitious composites) produced with ground granulated blast furnace slag. Cem Concr Res 37(7):1096–1105
15. European Committee for Standardization CEN EN 197-1 (2000) Cement—Part 1: composition, specifications and conformity criteria for common cements
16. Qian S, Li VC (2007) Simplified inverse method for determining the tensile strain capacity of strain hardening cementitious composites. J Adv Concr Tech 5(2):235–246
17. Yang EH, Yang Y, Li VC (2007) Use of high volumes of fly ash to improve ECC mechanical properties and material greenness. ACI Mater J 104(6):620–628
18. Maalej M, Li VC (1994) Flexural/tensile strength ratio in engineered cementitious composite. ASCE J Mater Civ Eng 6(4):513–528
19. Li VC (2003) On engineered cementitious composites (ECC). J Adv Concr Tech 1(3):215–230
20. Oner M (2000) A study of intergrinding and separate grinding of blast furnace slag cement. Cem Concr Res 30(3):473–480